J Mater Sci (2010) 45:3851–3857
DOI 10.1007/s10853-010-4440-5

Structure and photoluminescence properties of ZnS nanowires sheathed with SnO_2 by atomic layer deposition

Kyungjoon Baek · Changhyun Jin · Jungkeun Lee · Bong-Yong Jeong · Wan In Lee · Chongmu Lee

Received: 4 January 2010 / Accepted: 23 March 2010 / Published online: 3 April 2010

Abstract Influence of the thermal annealing atmosphere on the photoluminescence properties of ZnS-core/SnO_2-shell coaxial nanowires was investigated. ZnS nanowires were synthesized by a two-step process: the thermal evaporation of ZnS powders and the atomic layer deposition of SnO_2. Transmission electron microscopy and X-ray diffraction analyses reveal that two crystalline ZnS phases: one with a zinc blende structure and the other with an wurtzite structure coexist in the cores whereas the SnO_2 cores in the as-prepared coaxial nanowires are amorphous. The SnO_2 shells are found to be crystallized by thermal annealing. Photoluminescence (PL) measurements at room temperature show that the green emission of the ZnS/SnO_2 coaxial nanowires is enhanced in intensity by thermal annealing regardless of the annealing atmosphere. The PL emission is more significantly enhanced in intensity by annealing in a reducing atmosphere than in an oxidative atmosphere since Au_{Zn}^{-} is more easily generated in the ZnS cores in the former atmosphere.

K. Baek · C. Jin · J. Lee · C. Lee (✉)
Department of Materials Science and Engineering, Inha University, Incheon 402-751, South Korea
e-mail: cmlee@inha.ac.kr

B.-Y. Jeong
Bio-IT Convergence Center, Korea Institute of Ceramic Engineering and Technology, 103 Fashion Danji-gil, Geumcheon-gu, Seoul 153-801, South Korea

W. I. Lee
Department of Chemistry, Inha University, Incheon 402-751, South Korea

Introduction

In recent years, coaxial one-dimensional (1D) nanostructures consisting of cores and shells have been studied extensively on account of their interesting properties and potential applications in electronics and optoelectronics. In particular, coaxial 1D nanostructures consisting of different materials in the radial direction has potential applications in electronic and optoelectronic device applications owing to a couple of important reasons [1–9]. One is that the coaxial 1D nanostructures can realize various tailor-made functions by fabricating heterojunction nanodevices or depositing multilayers with different chemical compositions in the radial direction. Another is that we can not only avoid crosstalking between the building blocks of complex nanoscale circuits, but also protect them from contamination and oxidation. Passivation also offers many advantages such as substantial reduction of surface densities, prevention of the surface from adsorption of unwanted species, prevention of unnecessary charge injection, and partial screening of the external fields. In particular, passivation of nanowires is required in fabrication of field effect transistors and sensor devices based on nanowires. Much more work has been done for the latter purpose by coating the semiconductor cores with oxide materials, but there are few reports on the work for the former purpose yet. Here in this work, we focus on the former purpose. The properties of as-synthesized nanostructures can be modified or improved by selecting a proper coating material. Zinc sulfide (ZnS)-core/Tin oxide (SnO_2)-shell 1D nanostructures, which will be called ZnS/SnO_2 coaxial nanowires hereafter, are investigated to give an insight in tailoring the optical properties of ZnS nanowires.

ZnS has received significant attention over the past few decades since it is an important II–VI semiconductor with a

wide direct band gap (3.7 eV) at room temperature. ZnS has a wide variety of potential applications such as flat panel displays, infrared windows, ultraviolet light-emitting diodes and injection lasers, phosphors in cathode-ray tubes, electroluminescent thin film devices, and sensors owing to its intense luminescence, high refractive index, and high transmittance properties in the visible range [10, 11]. ZnS is also promising for room temperature exciton devices since it has large exciton binding energy (38 meV) compared with the room temperature thermal energy (25 meV) [12]. Various techniques for synthesis of ZnS nanowires have been reported. These techniques include thermal evaporation of ZnS powders [13], solvothermal process [14], chemical vapor deposition [10], electrochemical deposition [15], and template-assisted routes [16], etc. On the other hand, the optical properties of SnO_2 materials have also been widely investigated because of its key role in the injection process of a photochemical solar cell with high conversion efficiency [17, 18]. SnO_2 1D nanostrucureses have also been intensively synthesized in recent years. However, there has been no report yet on the synthesis and PL properties of ZnS/SnO_2 coaxial nanowires. In this paper, we report on the successful synthesis of ZnS/SnO_2 coaxial nanowires and influence of SnO_2 coating and thermal annealing on their PL properties. We have chosen the atomic layer deposition (ALD) technique to sheath the ZnS wires with SnO_2 since ALD is widely known to be a film deposition technique offering excellent thickness uniformity.

Experimental procedure

The experimental apparatus used for synthesizing ZnS nanowires is a two-heating zone horizontal tube-furnace the schematic diagram of which is shown elsewhere [9]. ZnS powders and Au-coated Si (100) were, respectively, used as a source material and the substrate for growth of ZnS nanowires. First, an Au thin film 3-nm thick was deposited onto the Si-substrate by using a RF magnetron sputtering system to prepare the Au-coated Si (100) substrate. Zn powders in an alumina boat and the Si-substrate were placed separately in the two-heating zone-tube furnace, where the Zn powders were in the first heating zone (Zone A) and the Si-substrate in the second heating zone (Zone B). The substrate temperatures of Zones A and B were set to 1000 and 850 °C, respectively, with the ambient nitrogen gas pressure and flow rate kept at 0.5 Torr and 500 standard cubic centimeters per minute (sccm), respectively, all through the synthesis process. The thermal evaporation process was conducted for 1 h and then the furnace was cooled down to room temperature. Next, ZnS/SnO_2 coaxial nanowire samples were prepared by ALD of SnO_2 thin films on the as-synthesized ZnS nanowires. $SnCl_4$ and H_2O, which were used as the precursors for Sn and an oxidant, respectively, were kept in a canister at 0 °C for $SnCl_4$ and 10 °C for H_2O. $SnCl_4$, H_2O, and N_2 purge gas was fed into the chamber through separate inlet lines and nozzles and purged in an ALD cycle. This cycle was repeated for 600 times. The typical pulse times for both the $SnCl_4$ and H_2O feeds were 1 s, and the purge time between the reactants was 2 s. The other process parameters for SnO_2 deposition used in these ALD processes are as follows: base vacuum $= 1.0 \times 10^{-6}$ Torr, chamber pressure $= 0.1$ Torr, N_2 gas flow rate $= 100$ sccm, and substrate temperature $= 350$ °C. Subsequently, the prepared ZnS/SnO_2 coaxial nanowires were annealed at 650 °C for 30 min in an Ar, O_2, or N_2—3 mol% H_2 atmosphere.

The as-synthesized and annealed coaxial nanowire samples were then characterized using glancing angle (0.5°) X-ray diffraction (XRD, X'pert MPD-Philips with Cu-K_α radiation), scanning electron microscopy (SEM, Hitachi S-4200), and transmission electron microscopy (TEM, Phillips CM-200). The high resolution TEM (HRTEM) images and selected area electron diffraction (SAED) patterns were also taken on the same systems. PL measurements were carried out at room temperature in a PL spectrometer (Kimon, SPEC-14031 K, Japan) with a He–Cd laser line (325 nm) as the excitation source.

Results and discussion

Figure 1a shows the SEM image of the as-prepared ZnS/SnO_2 coaxial nanowires. The nanowires are quite straight and uniform in diameter. Most nanowires have diameters of a few tens of nanometers and lengths up to a few hundreds of micrometers. As regards the growth mechanism of the 1D nanostructures, there are two dominant mechanisms: vapor–liquid–solid (VLS) and vapor–solid (VS) mechanisms. It is generally known that the growth process of 1D nanostructure is dominated by kinetics rather than thermodynamics. Nanoscale 1D structures of oxides prepared by thermal evaporation can be grown using either VLS or VS mechanism depending on the kind of material and the process conditions. The VLS mechanism is generally dominated in the thermal evaporation process carried out with the aid of a metal catalyst. Nevertheless, the absence of a catalyst particle at the end of nanowires does not necessarily mean that the growth of the nanowires is governed by a VS process, especially for the oxide nanostructures. This is because, in some cases, the metal catalyst, which makes effect under the reaction condition, may be oxidized into the oxide tip with the same composition as the nanowires while the furnace was cooled down to room temperature. A metallic droplet playing a role of catalyst is generally found at the tip of the nanowire grown through

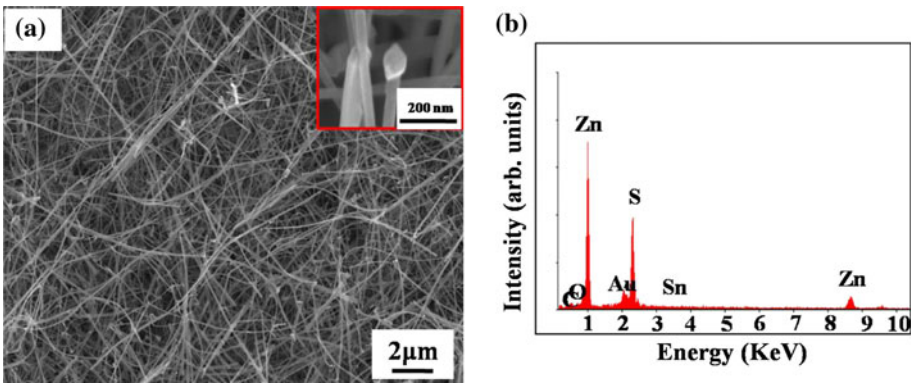

Fig. 1 **a** SEM image and **b** EDX spectrum of ZnS/SnO_2 coaxial nanowires synthesized by a two-step process: thermal evaporation of ZnS powders and ALD of SnO_2

VLS mechanism. It is widely accepted that nanowires can grow if only a droplet of the substrate metal acts as a catalyst and the diameter of the nanowires are uniform throughout the length of the nanowires through VLS mechanism even if no other metal were used as a catalyst. In the present work, an Au catalyst was used in our synthesis process of ZnS nanowires and the spherical droplets or particles are observed at the tips of nanowires in the inset of Fig. 1a. Figure 1b represents the energy-dispersive X-ray (EDX) spectra obtained from the tip of a typical ZnS/SnO_2 coaxial nanowire shown in the close-up pictures of the inset of Fig. 1a. The spectrum in Fig. 1b indicates that the particle at the tip of a typical coaxial nanowire comprises Au as well as Zn, Sn, S, and O elements. Therefore, we may say that both the SEM images and the EDX spectra support that the ZnS nanowires have been grown through conventional VLS mechanism in which an Au catalyst droplet is located at the growth front of each nanowire.

The structure and phase purity were examined by XRD. The XRD patterns of the as-synthesized and annealed ZnS/SnO_2 coaxial nanowires are shown in Fig. 2a and b, respectively. The reflection peaks for ZnS nanowires are indexed as the lattice planes of zinc blende (JCPDS 77-2100) and wurtzite ZnS structures (JCPDS 89-2158). The products appear to contain both zinc blende and wurtzite-structured ZnS phases. Of these two phases, the zinc blende ZnS phase may be a majority since the reflection intensities of the former is much stronger than that of the latter. On the other hand, no reflection peak for SnO_2 is observed in the XRD pattern of the as-synthesized nanowires, suggesting that the SnO_2 shells are amorphous before thermal annealing. Two small peaks of Au used as a catalyst for ZnS nanowires synthesis are also observed. On the other hand, several reflection peaks for SnO_2 as well as those for zinc blende ZnS and wurtzite ZnS are observed in the XRD pattern of the annealed nanowires, suggesting that SnO_2 shells have been crystallized by annealing.

Figure 3 is a low-magnification TEM image of a typical ZnS/SnO_2 coaxial nanowire annealed in an Ar atmosphere showing two segments: a thicker core ~40 nm thick and

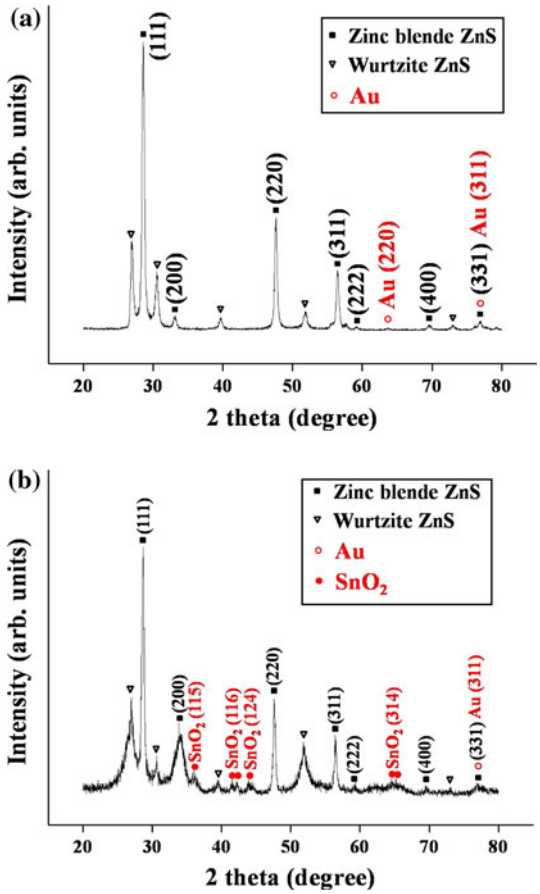

Fig. 2 XRD pattern of the ZnS/SnO_2 coaxial nanowires

thinner shell layers with an average thickness of ~20 nm on both sides of the core. The shell layers are not as uniform in thickness along the axial direction of the nanowires as is expected from the general characteristics of the film formed by ALD. We surmise at present that the nonuniformity of the shell layer thickness may be related to the crystallization of the SnO_2 layer during annealing although further systematic investigation is necessary. The HRTEM image of the interfacial area of the core and shell of a typical ZnS/SnO_2 coaxial nanowire and the corresponding

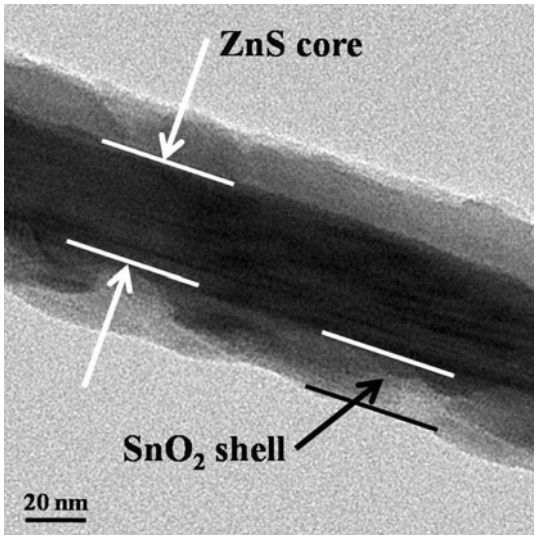

Fig. 3 Low-magnification TEM image of a typical ZnS/SnO_2 coaxial nanowire

SAED pattern are shown in Fig. 4a and b, respectively. The resolved spacing between the parallel fringes is about 0.31 nm, which is in good agreement with the interplanar distance of the {111} lattice plane families of zinc blende ZnS with a lattice parameter of $a = 0.5414$ nm (JCPDS 77-2100). Both the HRTEM image (Fig. 4a) and the associated SAED pattern taken along the $[1\bar{1}0]$ zone axis (the inset of Fig. 4a) clearly indicate that the ZnS core is crystalline. On the other hand, a fringe pattern is also clearly observable in the shell area of the annealed coaxial nanowire in the HRTEM image, which confirms that the SnO_2 shells have been crystallized by annealing since the SnO_2 shells in the as-prepared ZnS/SnO_2 coaxial nanowires were amorphous as we learned from their XRD pattern (Fig. 2). The resolved spacing between the parallel fringes in the shell area is about 0.24 nm, which is in good agreement with the interplanar distance of the {200} lattice plane families of orthorhombic SnO_2 with a lattice parameter of $a = 0.4737$ nm, $b = 5708$ nm, and $c = 1.5865$ nm (JCPDS 78-21063).

As regards the PL of ZnS nanowires, several PL emissions of ZnS 1D nanostructures have been reported before [19–28]. These emissions are largely classified into five different groups in terms of the wavelength range or the origin of the emission: near-band edge (NBE) emission in the range of 320–370 nm, violet emission in the range of 390–400 nm, blue emission in the range of 430–470 nm, green emission in the range 510–550 nm, and an orange

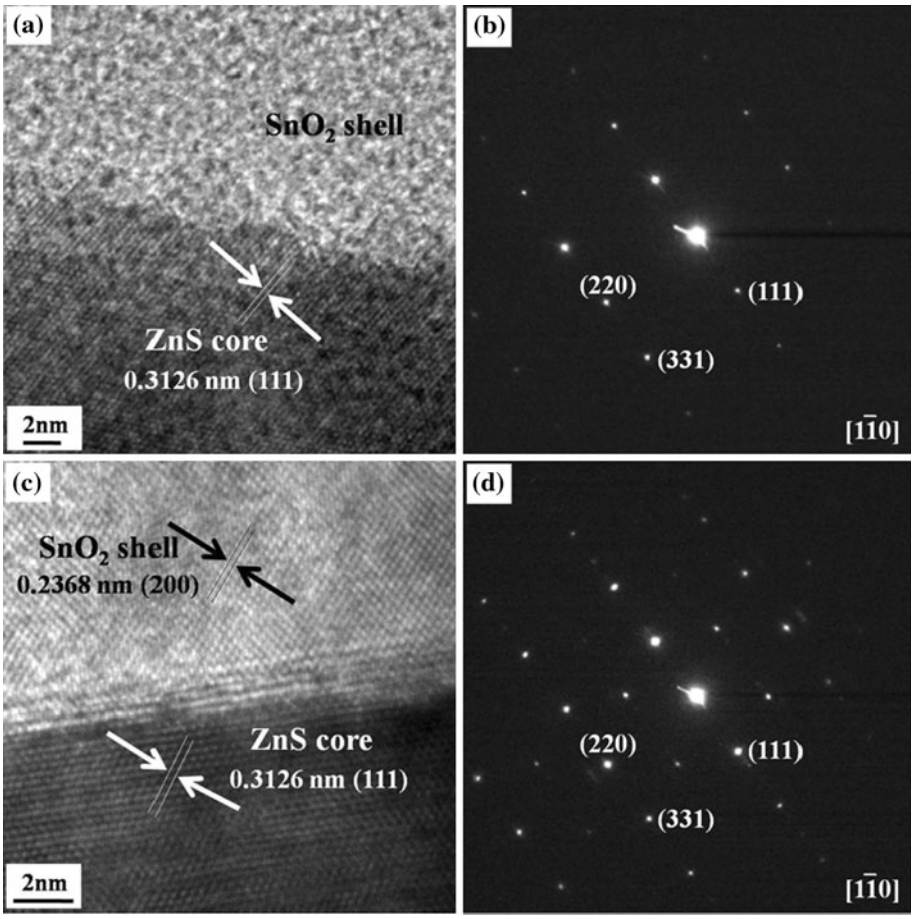

Fig. 4 **a** Local HRTEM image of a typical as-synthesized ZnS/SnO_2 coaxial nanowire at the core–shell interface region. **b** SAED pattern of the $[1\bar{1}0]$ zone axis of the nanomaterial at the same region as in (**a**). **c** Local HRTEM image of a typical annealed coaxial nanowire at the core–shell interface region. **d** SAED pattern of the $[1\bar{1}0]$ zone axis of the nanomaterial at the same region as in (**c**)

emission in the range of 600–620 nm. The NBE emission was reported for the wurtzite ZnS nanowires synthesized via vapor phase deposition [19] and solution routes [20]. The NBE emission is known to originate from band to band transitions since the band gap of ZnS (3.66 eV) corresponds to 330 nm [21]. The emission is, more concretely speaking, due to the excitonic transition [21] or the quantum size effect [22]. The violet emission is known to originate from deep levels like Zn^{2+} vacancies, interstitials, and dislocations [21, 22]. The blue emission was reported to be associated with the trapped luminescence arising from the surface states, Zn^{2+} vacancies, and S^{2-} vacancies [20, 23–28]. The green emission was reported to be attributed to dopants or impurity atoms, i.e., transitions from the conduction band of ZnS to the different levels of excited impurity atoms in the ZnS band gap [29, 30]. It was also suggested that a possible source for the green emission is Au^{+} ions substituting Zn^{2+} (Au_{Zn}^{-}) [31–33] resulting from Au diffusion from the Au thin film used to catalyze the nanowire growth [27, 34–36]. The orange emission is due to deep levels [24]. On the other hand, the PL property of SnO_2 was also reported by many researchers. The PL emission of bulk SnO_2 is known to be very weak at room temperature [37], but SnO_2 thin films were reported to show a broad emission peak near 396 nm [38]. A yellow emission peak was reported to be detected at 590 nm for SnO_2 powders [39]. The PL spectrum of the as-synthesized SnO_2 nanoribbons was reported to have two strong emission peaks at 392 and 439 nm and two weak ones at 486 and 496 nm, probably due to point defects [40]. There is also a report that the PL spectrum of the SnO_2 fishbone-like nanoribbons shows a strong green emission band centered at around 500 nm [41].

The PL measurements were carried out at room temperature with 325 nm excitation and the PL spectra of the as-synthesized and annealed ZnS nanowires are displayed in Fig. 5. A green emission band centered at around 515 nm is observed in either of the two PL spectra in this figure. This green emission may originate from S vacancies or the Au^{+} ions substituting Zn^{2+} (Au_{Zn}^{-}) in the ZnS core [31–33]. As-synthesized ZnS nanostructures commonly contain a large amount of S vacancies as they are Zn-rich [19–24]. We can also see that the PL emission of the ZnS nanowires is enhanced in intensity by thermal annealing. The enhancement in the PL emission intensity may be attributed to the increase in the concentration of S and Zn vacancies in the ZnS cores by thermal annealing. Vacancies form during the annealing process and many of them stay in the nanowires even after the nanowires are cooled down. In other words, the nanowires are supersaturated with vacancies, causing the PL emission enhancement.

The PL measurements of the ZnS/SnO_2 coaxial nanowires were also carried out at room temperature and the PL spectra of the nanowires annealed in different atmospheres along with that of the as-synthesized, i.e., unannealed ones are displayed in Fig. 6. A green emission band centered at around 515 nm is observed in all the PL spectra in this figure. The PL emission of ZnS/SnO_2 coaxial nanowires is enhanced in intensity by thermal annealing regardless of the annealing atmosphere, but annealing in a reducing atmosphere enhances the PL emission in intensity more significantly than annealing in an oxidative or inert gas atmosphere. As discussed above, the ZnS cores are supersaturated with vacancies after annealing, which may be the main cause for the enhancement in the green emission intensity. The influence of the annealing atmosphere, however, cannot be fully explained by changes in the vacancy concentrations.

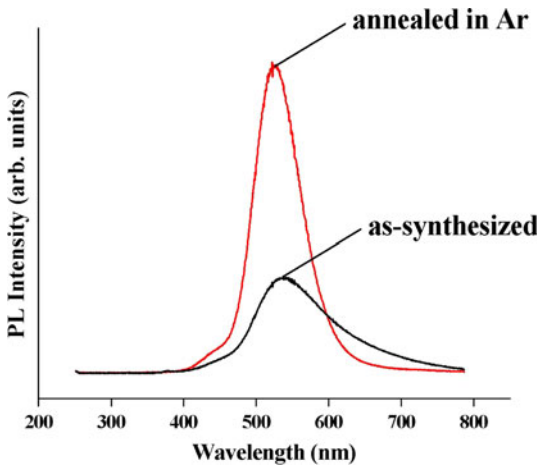

Fig. 5 Room temperature-PL spectra of the ZnS nanowires synthesized by thermal evaporation of ZnS powders and those annealed at 650 °C for 30 min in an Ar atmosphere

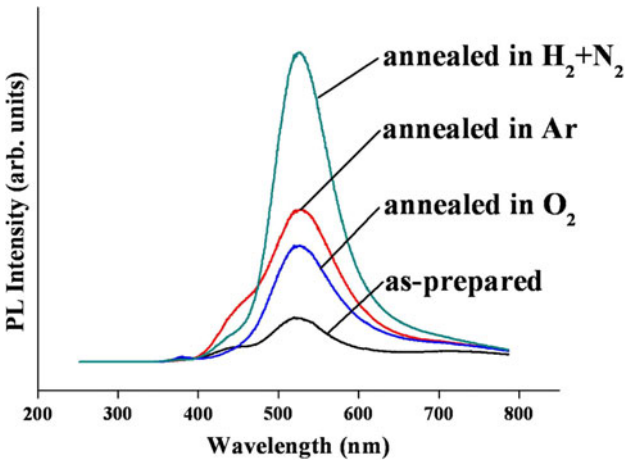

Fig. 6 Room temperature-PL spectra of the ZnS/SnO_2 coaxial nanowires annealed at 650 °C for 30 min in different atmospheres along with the as-prepared ZnS/SnO_2 coaxial nanowires

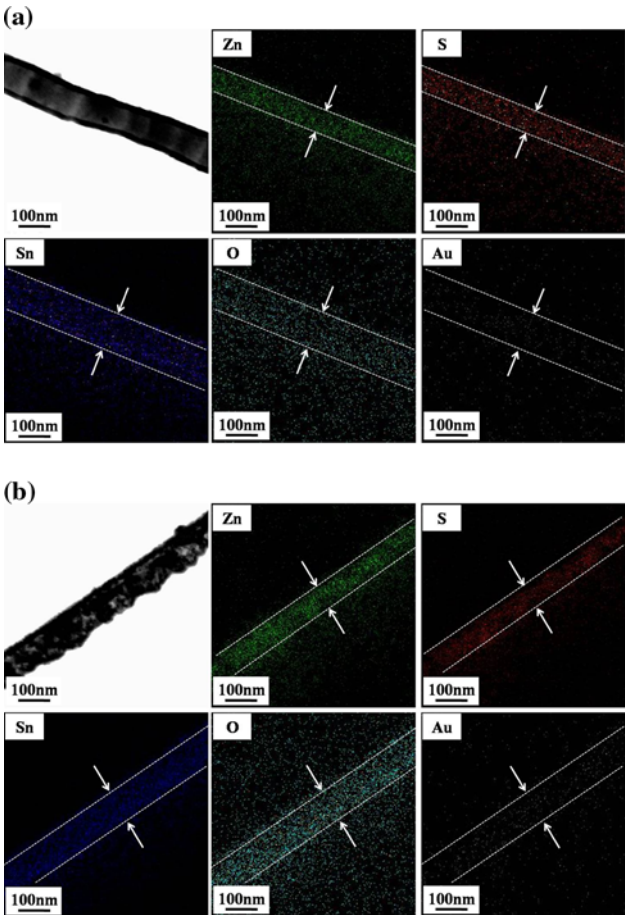

Fig. 7 EDX element mapping profiles of the ZnS/SnO_2 coaxial nanowires **a** as-prepared (unannealed) and **b** annealed in an Ar atmosphere

EDX spectroscopy analyses were performed to further investigate the origins of the PL emission enhancement in intensity by annealing. The EDX element mapping profiles for the as-synthesized and annealed ZnS/SnO_2 coaxial nanowire samples are shown in Fig. 7a and b, respectively. A close comparison of the Au mapping profiles in Fig. 7a and b indicates that the annealed nanowire has a higher density of the Au element than the as-synthesized one. The white spots distributed along the axial direction of the nanowires are Au atoms. Most of the Au atoms used as catalysts in the VLS growth exist at the tip of the as-synthesized nanowire as was shown in Fig. 1a although the tip area is not shown in Fig. 7a. The Au atoms located at the tip of the nanowire may be redistributed in the thermal annealing process. Diffusion of Au atoms along the axial direction of the nanowire occurs during annealing, which results in a decrease in the Au concentration at the tip but an increase in the Au concentration in the other areas of the nanowire. This does not necessarily mean that the Au_{Zn}^- concentration in the core is increased in the other areas of the nanowire by annealing, but we can easily guess that the probability of substitution of Au^+ ions with Zn^{2+} will be increased by annealing. As written above, Au_{Zn}^- is also a possible source for the green emission [31–33]. At present, it is, however, not well understood why the Au_{Zn}^- concentration in the core is further increased by annealing in a reducing atmosphere compared to annealing in an oxidative atmosphere. Further study is necessary, but we surmise at the moment that the enhanced substitution of Zn atoms with Au atoms is associated with the higher concentration of S vacancies in the nanowires annealed in a reducing atmosphere. The unstable Zn atoms with dangling bonds due to neighboring S vacancies are more likely to be substituted by Au atoms.

Conclusions

A crystalline ZnS phase with a zinc blende structure and a crystalline ZnS phase with an wurtzite structure coexist in the cores of the ZnS/SnO_2 coaxial nanowires synthesized by using a two-step process: thermal evaporation of ZnS powders and ALD of SnO_2 has been investigated, whereas the SnO_2 cores in the as-prepared coaxial nanowires are amorphous. The SnO_2 shells are found to be crystallized by thermal annealing. The ZnS/SnO_2 coaxial nanowires have a green emission band centered at around 515 nm originated from Au^+ ions substituting Zn^{2+} (Au_{Zn}^-) in the ZnS core. The green emissions of both the ZnO nanowires and the ZnS/SnO_2 coaxial nanowires are enhanced in intensity by thermal annealing due to the formation of Au_{Zn}^- as well as Zn and S vacancies. Annealing in a reducing atmosphere enhances the PL emission in intensity more significantly than annealing in an oxidative atmosphere since the former generates a higher concentration of Au_{Zn}^- in the ZnS core than the latter.

Acknowledgements This work was financially supported by Korean Science and Engineering Foundation (KOSEF) through the 2007 National Research Laboratory (NRL) Program.

References

1. Morales AM, Lieber CM (1998) Science 279:208
2. Kim HW, Shim SH, Lee C (2004) Mater Sci Eng B 111:131
3. Yu Y, Xiang J, Yang C, Lu W, Lieber CM (2004) Nature 450:61
4. Lauhon LJ, Gudiksen MS, Wang D, Lieber CM (2002) Nature 420:57
5. Choi HJ, Johnson JC, He R, Lee SK, Kim F, Pausauskie P, Goldberger J, Saykally RJ, Yang P (2003) J Phys Chem B 107:8721
6. Kim HW, Shim SH, Lee C (2007) Mater Sci Eng B 136:148
7. Park S, Kim H, Lee JW, Kim HW, Lee C (2008) J Kor Phys 53:657
8. Park S, Jun J, Kim HW, Lee C (2009) Solid State Comm 149:315
9. Jun J, Jin C, Kim H, Kang J, Lee C (2009) Appl Phys A 96:813

10. Prevenslik TV (2000) J Lumin 1210:87
11. Yamamoto T, Kishimoto S, Lida S (2001) Physica B 308:916
12. Biswas S, Ghoshal T, Kar S, Chakrabarti S, Chaudhuri S (2008) Crystal Growth Design 8:2171
13. Li YQ, Zou K, Shan YY, Zapien JA, Lee ST (2006) J Phys Chem B 110:6759
14. Chai L, Du J, Xiong S, Li H, Zhu Y, Qian Y (2007) J Phys Chem C 111:12658
15. Xu XJ, Fei GT, Yu WH, Wang XW, Chen L, Zhang LD (2006) Nanotechnology 17:426
16. Shen XP, Han M, Hong JM, Xue ZL, Xu Z (2005) Chem Vap Dep 11:250
17. Liu Y, Zheng C, Wang W, Zhau Y, Wnag G (2001) J Crystal Growth 233:8
18. Xu C, Xu G, Liu Y, Zhao X, Wang G (2002) Scr Mater 46:789
19. Chang Y, Wang M, Chen X, Ni S, Qiang W (2007) Solid State Comm 142:295
20. Zhang J, Yang Y, Jiang F, Li J, Xu B, Wang X, Wang S (2006) Nanotechnology 17:2695
21. Becker WG, Bard AJ (1983) J Phys Chem 87:4888
22. Shionoya S (1966) In: Goldberg P (ed) Luminescence of inorganic solids. Academic Press, New York, p 205
23. Bol AA, Meijerink A (2001) J Phys Chem B 105:10203
24. Hu P, Liu Y, Fu L, Cao L, Zhu D (2004) J Phys Chem B 108:936
25. Denzler D, Olschewski M, Sattler K (1998) J Appl Phys 84:2841
26. Zhu YC, Bando Y, Xue DF (2003) Appl Phys Lett 82:1769
27. Wang YW, Zhang LD, Liang CH, Wang GZ, Peng XS (2002) Chem Phys Lett 357:314
28. Kasai PH, Otomo Y (1962) J Phys Chem 87:4888
29. Jiang Y, Meng XM, Liu J, Xie ZY, Lee CS, Lee ST (2003) Adv Mater 15:323
30. Jiang Y, Meng XM, Liu J, Hong ZR, Lee CS, Lee ST (2003) Adv Mater 15:1195
31. Henderson ST, Ranby PW, Halstead MB (1959) J Electrochem Soc 106:27
32. Hoshina T, Kawai H (1980) Jpn J Appl Phys 19:267
33. Poolton NRJ (1987) J Phys C 20:5867
34. Li Q, Wang C (2003) Appl Phys Lett 83:359
35. Xiong Q, Chen G, Acord JD, Liu X, Zengei JJ, Gutierrez HR, Redwing JM, Lew Yan Voon LC, Lassen B, Eklund PC (2004) Nano Lett 4:1663
36. Rosenberg RA, Shenoy GK, Heigl F, Lee ST, Kim PSG, Zhou XT, Sham TK (2005) Appl Phys Lett 86:263115
37. Chowdhury PS, Saha S, Patra A (2004) Solid State Commun 131:785
38. Jeong J, Choi SP, Chang CJ, Shin DC, Park JS, Lee BT, Park YJ, Song HJ (2003) Solid State Commun 127:595
39. Chang SS, Yoon SO, Park HJ (2005) Ceram Int 31:405
40. Hu JQ, Ma XL, Shang NG, Xie ZY, Wong NB, Lee CS, Lee ST (2002) J Phys Chem B 106:3823
41. Hu JQ, Bando Y, Golberg D (2003) Chem Phys Lett 372:758